HHS Public Access

Author manuscript

Gastrointest Endosc. Author manuscript; available in PMC 2017 January 01.

Published in final edited form as:

Gastrointest Endosc. 2016 January ; 83(1): 107–114. doi:10.1016/j.gie.2015.06.045.

Quantitative analysis of high-resolution microendoscopic images for diagnosis of neoplasia in patients with Barrett's esophagus

Dongsuk Shin, PhD[1,5], **Michelle H. Lee, MD**[2], **Alexandros D. Polydorides, MD, PhD**[3], **Mark C. Pierce, PhD**[4], **Peter M. Vila, MD**[2,6], **Neil D. Parikh, MD**[2,7], **Daniel G. Rosen, MD**[8], **Sharmila Anandasabapathy, MD**[2], and **Rebecca R. Richards-Kortum, PhD**[1]

[1]Department of Bioengineering, Rice University, Houston, Texas

[2]Division of Gastroenterology, The Mount Sinai Medical Center, New York, New York

[3]Department of Pathology, The Mount Sinai Medical Center, New York, New York

[4]Department of Biomedical Engineering, Rutgers, The State University of New Jersey, Piscataway, New Jersey

[5]Department of Neurosurgery, The University of Texas Medical School at Houston, Houston, Texas

[6]Department of Otolaryngology-Head and Neck Surgery, Washington University School of Medicine, St. Louis, Missouri

[7]Division of Digestive Diseases, Yale-New Haven Hospital, New Haven, Connecticut

[8]Department of Pathology, Baylor College of Medicine, Houston, Texas

Abstract

Background and Aims—Previous studies show that microendoscopic images can be interpreted visually to identify the presence of neoplasia in patients with Barrett's esophagus, but this approach is subjective and requires clinical expertise. This study describes an approach for quantitative image analysis of microendoscopic images to identify neoplastic lesions in patients with Barrett's esophagus.

Corresponding author: Rebecca R. Richards-Kortum, Rice University, 6100 Main Street, Houston, TX 77005. Phone: 713-348-3823; Fax: 713-348-5877; rkortum@rice.edu.

The content is solely the responsibility of the authors and does not necessarily represent the official views of the National Cancer Institute, the National Institute of Biomedical Imaging and Bioengineering, or the National Institutes of Health.

Competing interests
None reported.

Author contributions: conception and design (DS, MHL, PMV, SA, RRR); analysis and interpretation of the data (DS, MHL, ADP, PMV, NDP, DGR); drafting of the article (DS, RRK); critical revision of the article for important intellectual content (DS, MCP, PMV, RRR); final approval of the article (SA, RRR).

Methods—Images were acquired from 230 sites in 58 patients using a fiber optic high-resolution microendoscope (HRME) during a standard endoscopic procedure. Images were analyzed by a fully automated image processing algorithm, which automatically selected a region of interest (ROI) and calculated quantitative image features. Image features were used to develop an algorithm to identify the presence of neoplasia; results were compared to histopathology diagnosis.

Results—A sequential classification algorithm that used image features related to glandular and cellular morphology resulted in a sensitivity of 84% and a specificity of 85%. Applying the algorithm to an independent validation set resulted in a sensitivity of 88% and a specificity of 85%.

Conclusions—This pilot study demonstrates that automated analysis of microendoscopic images can provide an objective, quantitative framework to assist clinicians in evaluating esophageal lesions from patients with Barrett's esophagus.

Introduction

Highly prevalent in the United States, Barrett's esophagus (BE) is a major risk factor for the development of esophageal adenocarcinoma (EAC). The incidence rate of EAC is rapidly increasing in the Western World, with an estimated 600% increase in incidence over the last 40 years [1–4]. Moreover, most cases of EAC are diagnosed at a late stage when treatment is challenging, resulting in significant morbidity and a poor 5-year survival rate [5]. Early diagnosis of neoplasia in patients with BE is challenging. Even with routine endoscopic surveillance, it is difficult to identify areas of dysplasia or neoplasia because they may be focal and flat and not visible on standard endoscopy. Endoscopy with random 4-quadrant biopsies is the accepted surveillance of BE for identifying the presence of dysplasia. However, 4-quadrant biopsies every 2 cm of the Barrett's mucosa sample only a small fraction of the entire segment of BE, which can range from 1 to 20 cm in length, often resulting in sampling error. Random biopsy protocols have been shown to miss greater than 50% of neoplasia [6, 7]. Improving early detection of BE-associated neoplasia is, therefore, critical to improve survival and quality of life for patients.

Coupled with standard endoscopy, high-resolution optical imaging technologies have the potential to improve diagnostic accuracy for the detection of precancerous and cancerous lesions in patients with BE by allowing real-time imaging with resolution that approaches that of conventional histopathology. Confocal endomicroscopy can distinguish esophageal neoplasia from benign Barrett's mucosa with high accuracy by providing images of tissue architecture and cellular morphology with subcellular resolution throughout the esophageal epithelium. In several studies, confocal endomicroscopy combined with high-definition white-light endoscopy (HD-WLE) was shown to significantly improve the ability to detect BE-associated neoplasia [8, 9]. In a study conducted by Sharma et al. the sensitivity and specificity were 68.3% and 87.8%, respectively, when confocal endomicroscopy was used in combination with HD-WLE, compared with 34.2% and 92.7%, respectively, for HD-WLE alone [9]. Despite the potential for improving detection of esophageal neoplasia, current confocal platforms are available mostly in tertiary referral centers due to high-cost ($150,000–$300,000). We recently developed a low-cost (<$5000) fiber-optic high-

resolution microendoscope (HRME), capable of imaging tissue with subcellular resolution comparable to confocal microendoscopy [10]. Muldoon et al. showed the feasibility of the HRME to image various esophageal tissue types, including squamous, BE, and high-grade dysplastic tissue obtained by endoscopic mucosal resection [11]. Pierce et al. demonstrated the ability of the HRME to differentiate high-grade dysplasia from normal squamous mucosa and BE without dysplasia in vivo from a patient with BE [12].

Most studies of high-resolution endoscopic imaging rely on subjective visual interpretation. Inter- and intra-observer variability in the assessment of images impairs reliable diagnosis. Quantitative analysis offers an objective manner to examine images; the use of computer-aided algorithms may reduce subjectivity among reviewers and enhance reproducibility, resulting in improving diagnostic accuracy. Such algorithms can be coupled with advanced optical imaging techniques with the potential to allow real-time in vivo diagnosis with high accuracy. The aim of this study was to develop quantitative HRME image analysis criteria for delineation of esophageal neoplasia in patients with BE.

Methods

Patients

Patients with known BE or Barrett's with dysplasia who were scheduled for routine surveillance endoscopy within an academic gastroenterology practice in New York City or who were referred from outside hospitals were recruited for this study. Study participants were at least 18 years old and signed a written informed consent and authorization. Persons who have allergy to proflavine, active GI bleeding, and contraindication to endoscopy were excluded from the study. The study was reviewed and approved by the Institutional Review Boards at Mount Sinai Medical Center and Rice University. The study was registered on Clinicaltrials.gov (registration number NCT01384227 and NCT02018367).

An endoscopist performed a standard upper endoscopic examination. Areas of Barrett's mucosa suspicious for neoplasia during endoscopy were further interrogated with the HRME. Before HRME imaging, a topical solution (1–2 mL) of 0.01% proflavine in sterile PBS was applied to the esophageal surface using a standard endoscopic spray catheter. Proflavine, which was used under an Investigational New Drug (IND) application from the Food and Drug Administration (IND 102 217), is a fluorescent contrast agent which stains cell nuclei [13]. After application of proflavine, the fiber-optic probe of the HRME was inserted through the biopsy channel of the endoscope, and the distal tip was placed in gentle contact with the mucosal surface. Real-time imaging was performed; at each site, video sequences of approximately 3 seconds duration were acquired and then saved to a file. HRME images also were obtained from at least 2 of 4 sites selected for random quadrant biopsy. At each site imaged with the HRME, the fiber probe was used to make a superficial dimple to "mark" the imaged area. Each imaged site was then biopsied and submitted for routine histologic diagnosis. The endoscopist completed a standard of care evaluation by taking the remaining biopsies of the routine 4-quadrant biopsy procedure and submitting these for routine histologic diagnosis. All of the specimens were processed and sectioned in a standardized manner. Slides were later reviewed by 2 expert gastrointestinal pathologists (A.P., D.R.) blinded to both the endoscopists' clinical impressions as well as the HRME

images. Cohen's kappa statistic was used to assess the agreement of the pathologists. Diagnosis was performed using standard histologic criteria [14]; based on consensus histologic diagnosis as the criterion standard, samples were divided into the following categories: squamous mucosa, gastric cardia, Barrett's metaplasia, low-grade dysplasia (LGD), high-grade dysplasia (HGD), or adenocarcinoma. Squamous mucosa, gastric cardia, Barrett's metaplasia, and LGD were considered to be non-neoplastic, whereas the remaining categories were considered neoplastic.

Imaging System

The HRME system has been previously described in detail [15]. A bandpass-filtered blue light emitting diode (LED) (FF01-452/45, Semrock, Rochester, NY; M455L2, Thorlabs, Newton, NJ) provides light that passes through a dichroic mirror (485DCLP, Chroma Technology Corp, Bellows Falls, Vt) onto a fiber bundle (FIGH-30-850N, Fujikura, Tokyo, Japan) with a 1-mm outer diameter that is placed in contact with the tissue surface to be imaged. The fiber bundle is composed of 30,000 optical fibers with a 4-μm center-to-center spacing and a 720-μm field of view (FOV). Fluorescence emission returns through the fiber bundle and is imaged through the dichroic mirror and a 550-nm bandpass filter (FF03-550/88, Semrock, Rochester, NY). The emission then passes onto the optical sensor of a charge-coupled device (CCD) camera (GRAS-14S5M, Point Grey, Richmond, Canada). The system has a lateral and axial resolution of 4.4 and 20 μm, respectively. A laptop computer controls the system obtains and displays video at a rate of 15 frames per second.

Flowchart for Visual Classification of HRME Images of the Esophagus

HRME images were reviewed for quality control (QC) purposes by two reviewers (RRK, ML). First, one reviewer (ML) identified a single representative image frame from each video sequence. Second, the images selected from each video were then reviewed independently for QC by the two reviewers who were blinded to clinical impression and histologic diagnosis. Images were rejected if at least 50% of the FOV was out of focus or showed evidence of motion artifact. Last, images that met QC were then reviewed for the selection of a single image with the best image quality per site.

Two reviewers familiar with HRME images of BE from prior studies [12, 16] were asked to classify each image acquired in this study as neoplastic or non-neoplastic. They were blinded to histopathology diagnosis. To assist in the classification, each image was printed on a 3″×5″ card and reviewers independently arranged cards according to classification. Reviewers were interviewed after the exercise to allow the investigators to understand the rules they used in classification. A flowchart was then created to represent the sequential classification steps followed in reaching a visual assessment. The flowchart consisted of decision nodes structured in the form of "yes" or "no" questions that led to a specific answer choice. Each question was chosen to describe differences in cell type, cell morphology, and glandular structures, subsequently leading to each diagnostic category, and then used to extract relevant image features for the following classification analysis.

We also evaluated whether this flowchart could aid endoscopists in making correct visual reads with HRME images of the esophagus. The digital HRME images were reviewed by

three endoscopists with HRME experience. Using the flowchart, reviewers analyzed the entire set of images and recorded an impression for each image as one of the five categories. Results of visual image interpretation using the flowchart were calculated for each reviewer.

Automated Image Analysis

Figure 1 illustrates the quantitative image analysis procedure used in this study. At each image, the whole circular FOV was selected for analysis. Low-pass Gaussian filtering was applied to remove the background pattern associated with the structure of the fiber bundle used for HRME imaging [17]. Because the images acquired in this study exhibited different morphologic structures associated with squamous epithelium, intestinal metaplasia, and neoplasia, a variety of image features were explored for possible use in a classification algorithm. First, image intensity was calculated as a feature that could potentially be used to separate squamous tissue from glandular tissue because the fluorescence intensity of glands might be higher than that of squamous cell nuclei. Second, images were segmented to identify cell nuclei. Morphologic image processing and thresholding were used to segment nuclei in each HRME image. Morphologic processing (opening and smoothing) was used to compensate for the nonuniform background. Once a threshold was chosen by the histogram-based automated thresholding method, nuclear and cytoplasmic regions were separated by this threshold. After nuclear segmentation, nuclear-to-cytoplasmic area ratio (N/C ratio), mean nuclear size, and mean nearest internuclear distance were calculated for each image. Last, granulometry was used to characterize epithelial thickness and lumen size of glands, in addition to nuclear size. Granulometry is a morphologic method to calculate the size distribution of objects in an image without explicitly segmenting each object [18]. HRME images exhibit bright nuclei and epithelial layers along with dark glandular lumens. The size distribution of nuclei and epithelial layers was calculated from each HRME image. Similarly, the size distribution of glandular lumens was calculated from the complement of each HRME image. From granulometry, the most frequent size, kurtosis, and skewness of the distribution of the following features were computed for each image: epithelial thickness and glandular lumen size.

Automated Image Classification

Features extracted from the HRME images were then used to develop and evaluate an automated sequential classification algorithm to classify whether each imaged site contained neoplastic tissue (HGD or cancer) or was non-neoplastic (normal squamous mucosa, gastric cardia, Barrett's metaplasia, or LGD). Each step of the classification algorithm was modeled after the corresponding decision node of the flowchart developed from visual assessment. Two-class linear discriminant analysis was used to develop a classification algorithm at each node; extracted image features were added one at a time until classification performance no longer improved. Sensitivity and specificity were calculated for the sequential classification algorithm using histologic diagnosis as the gold standard. Data obtained at The Mount Sinai Medical Center from February 2nd, 2009 to July 28th, 2011 were assigned to a training set to develop and optimize the algorithm. The data obtained at The Mount Sinai Medical Center from September 27, 2012 to November 21, 2014 were assigned to an independent validation set to assess algorithm performance. Image analysis and classification are fully automated and require a total of 52 seconds for a single image.

Results

Subject Information: Patients and Sites

A total of 93 subjects were enrolled in this study; corresponding pathology was available from 317 biopsy sites in 61 patients with images. Only sites with corresponding pathology results were considered for analysis. The agreement between the pathologists was found to be substantial, with a kappa statistic of 0.75. Consensus diagnosis was reached upon subsequent review for the study. Two reviewers (RRK, ML) selected representative HRME images from 230 sites that passed QC review; 87 sites had no images that passed QC review. The remaining data set for subsequent analysis consisted of 230 images from 230 sites in 58 patients. Of these sites, 195 were diagnosed as non-neoplastic and 35 were diagnosed as neoplastic. The data obtained from February 2, 2009 to July 28, 2011 were assigned to a training set which consisted of 77 images from 77 sites in 31 patients. The remaining data obtained from September 27, 2012 to November 21, 2014 were assigned to an independent validation set which consisted of 153 images from 153 sites in 27 patients. Table 1 shows the histologic diagnosis of the measured sites available for further analysis.

Visual Interpretation with Flowchart

Figure 2 shows the sequential flowchart that was developed for visual classification. Images from the training set were categorized into one of the following categories: normal squamous mucosa, gastric cardia, Barrett's metaplasia, or neoplastic. Observers were first asked whether glands were visible in the HRME image. If not, images were classified as neoplastic if nuclei were crowded and as normal squamous tissue if nuclei were not crowded. If glands were visible, the epithelial layer was thin, and the lumen was large, the images were classified as gastric cardia. If not, the observers were asked whether the glandular epithelium shows loss of regular architecture. Images with regular glandular architecture were classified as Barrett's metaplasia, whereas those with loss of regular architecture were classified as neoplastic.

Using the sequential flowchart, 3 endoscopists performed visual image classification, resulting in an average sensitivity of 81% (95% confidence interval (CI), 73%–88%) and an average specificity of 76% (95% CI, 50%–100%), with a kappa statistic of 0.39, indicating fair agreement.

Classification Performance

Quantitative image features were calculated. Relevant image features were selected as described to develop a sequential classification algorithm with optimal performance. Figure 3A and 3B illustrate the resulting classification tree of the training and validation sets and show the performance of each node in the tree. At Node 1 of the classification tree, the most frequent epithelial thickness and intensity of the epithelial layer were chosen to classify whether each image contained glandular tissue or not. At Node 2, the N/C ratio was chosen to classify each image as neoplastic or non-neoplastic squamous tissue. The most frequent lumen size and kurtosis of lumen size were chosen at Node 3 to classify each image as cardia or not. The skewness of epithelial thickness was chosen at Node 4 to classify each image as neoplastic or non-neoplastic glandular tissue. Using the sequential classification

algorithm in the training set, 16 of 19 sites were correctly classified as neoplastic, and 49 of 58 sites were correctly classified as non-neoplastic, resulting in a sensitivity of 84% and a specificity of 85%. Applying the algorithm to the validation set resulted in a sensitivity of 88% and a specificity of 85%; 14 of 16 sites were correctly classified as neoplastic, and 116 of 137 sites were correctly classified as non-neoplastic.

Discussion

In this study, we demonstrated that HRME imaging could discriminate BE with neoplasia from benign esophageal tissue including normal squamous, BE without dysplasia, and BE with low-grade dysplasia using quantitative image analysis and sequential classification analysis. A classification algorithm was created by sequential analysis of image features within the images, which represented differences in tissue architecture and cellular morphology between non-neoplastic and neoplastic esophageal tissue. The sequential classification algorithm was able to distinguish between neoplastic and neoplastic tissue with a sensitivity of 84% and a specificity of 85%. Preservation and Incorporation of Valuable Endoscopic Innovations thresholds suggested by the guidelines developed by The American Society for Gastrointestinal Endoscopy are a per-patient sensitivity of 90% or greater, specificity of 80% or greater, and negative predictive value (NPV) of 98% or greater [19]. Due to the small number of patients enrolled in the present study, we performed per-biopsy analysis. Our classification algorithm resulted in a sensitivity of 88%, specificity of 85%, and NPV of 98% in an independent validation set. Given the results an estimated NPV would be sufficiently high in a low prevalence setting, but results must be confirmed in a larger data set to support the use of HRME with quantitative image analysis as an appropriate approach for imaging of BE.

In several studies with confocal endomicroscopy, confocal imaging criteria for BE neoplasia were established and evaluated. Pohl et al. [20] evaluated the use of confocal endomicroscopy in the detection of neoplasia in 296 sites from 38 patients with BE, and achieved a sensitivity of 80% and a specificity of 94.1%, with a corresponding negative predictive value of 98.9%. Similarly, in a study conducted by Gaddam et al. [21], confocal imaging criteria for dysplastic BE were established and evaluated using 50 confocal images, resulting in a sensitivity of 76% and a specificity of 85%. Wallace et al. [22] established confocal imaging criteria in a training set of 20 BE images and tested in an independent validation set of 20 BE images. The study reported a sensitivity of 88% and a specificity of 96%. Confocal endomicroscopy has shown high accuracy for detection of neoplasia; however, inter- and intra-observer variability exist in the interpretation of images obtained with this technique [23–25]. Rigorous diagnostic criteria using quantitative image analysis can reduce this subjectivity and provide consistent diagnosis with high accuracy. Muldoon et al. developed quantitative image analysis criteria for HRME images from either endoscopically resected or biopsied tissue to distinguish between neoplastic and non-neoplastic esophageal mucosa [16]. The quantitative analysis using textural features within the images achieved a sensitivity of 87% and a specificity of 85%, whereas human analysis for the same images achieved average sensitivity and specificity of 87% and 53%, respectively.

The quantitative classification algorithm described in this paper has the potential to improve the accuracy and reproducibility for detection of esophageal neoplasia by providing an objective means to classify images with improved consistency. This approach may be of use to clinicians, especially in low-resource settings. Also, it is noted that this sequential classification algorithm used intuitive images features which corresponded well to ones used for visual interpretation of the HRME images, such as epithelial cell morphology and glandular architecture of BE.

Several other studies have also proposed quantitative analysis of HRME images for diagnosis of neoplasia in patients with oral neoplasia [26, 27], cervical neoplasia [28, 29], and esophageal squamous cell carcinoma [30]. Analysis used in these studies, however, used nuclear segmentation to distinguish differences in cell morphology of neoplastic tissue. It is difficult to extend this approach to analysis of images from patients with neoplasia in the glandular epithelium, which exhibits differences in not only nuclear morphology but also glandular architecture [12, 31]. The quantitative classification algorithm presented here could be applied to any analysis of HRME images of the glandular epithelium where a variety of tissue types exist. Furthermore, confocal imaging of the gastrointestinal epithelium could be advantaged by this quantitative sequential classification analysis.

A limitation of this study is the small field of view (720 μm in diameter) of the HRME. Often, dysplastic changes in BE occur focally; the HRME may not image the small area of dysplasia identified in the larger biopsy specimen. The solution to this limitation could be to use video mosaicing during imaging, which is an emerging technique to increase the acquired field of view [32]. Another limitation is that 30% of sites were excluded due to bad image quality by because they were out of focus or had motion artifact. Technical improvements in the frame rate of imaging devices may minimize motion artifact during future image acquisition. Also, the current algorithm requires a total of 52 seconds to process and classify an image, which limits the ability to perform automated analysis at the time of endoscopy. Further improvements in execution speed may enable an automated frame-by-frame analysis.

The use of the HRME and quantitative diagnostic algorithm presented here could potentially impact the application of high-resolution microendoscopy as a useful tool in clinical practice by providing a cost-effective and reliable method for assisting clinicians in detecting esophageal neoplastic lesions during endoscopy. Further evaluation of this classification algorithm in real-time will be necessary in clinical practice.

Acknowledgments

Research reported in this publication was supported by the National Cancer Institute of the National Institutes of Health under Award Number R01CA140257 and the National Institute of Biomedical Imaging and Bioengineering under Award Number R01EB007594.

Acronyms

HRME	high-resolution microendoscope

BE	Barrett's esophagus
EAC	esophageal adenocarcinoma
HD-WLE	high-definition white-light endoscopy
IND	investigational new drug
LGD	low-grade dysplasia
HGD	high-grade dysplasia
LED	light emitting diode
FOV	field of view
CCD	charge-coupled device
QC	quality control
N/C ratio	nuclear-to-cytoplasmic ratio
CI	confidence interval

References

1. Ferlay J, Shin HR, Bray F, et al. GLOBOCAN 2008. Int J Cancer. 2010; 127:2893–917. [PubMed: 21351269]
2. Jemal A, Bray F, Center MM, et al. Global Cancer Statistics. CA Cancer J Clin. 2011; 61:69–90. [PubMed: 21296855]
3. Pohl H, Welch HG. The role of overdiagnosis and reclassification in the marked increase of esophageal adenocarcinoma incidence. J Natl Cancer Inst. 2005; 97:142–6. [PubMed: 15657344]
4. Siegel R, Naishadham D, Jemal A. Cancer statistics, 2013. CA Cancer J Clin. 2013; 63(1):11–30. [PubMed: 23335087]
5. Wang KK, Sampliner RE. Updated guidelines 2008 for the diagnosis, surveillance and therapy of Barrett's esophagus. Am J Gastroenterology. 2008; 103:788–97.
6. Vieth M, Ell C, Gossner L, et al. Histological analysis of endoscopic resection specimens from 326 patients with Barrett's esophagus and early neoplasia. Endoscopy. 2004; 36:776–81. [PubMed: 15326572]
7. Reid BJ, Blount P, Feng Z, et al. Optimizing endoscopic biopsy detection of early cancers in Barrett's high-grade dysplasia. Am J Gastroenterol. 2000; 95:3089–96. [PubMed: 11095322]
8. Kiesslich R, Gossner L, Goetz M, et al. In vivo histology of Barrett's esophagus and associated neoplasia by confocal laser endomicroscopy. Clin Gastroenterol Hepatol. 2006; 4:979–87. [PubMed: 16843068]
9. Sharma P, Meining AR, Coron E, et al. Real-time increased detection of neoplastic tissue in Barrett's esophagus with probe-based confocal laser endomicroscopy: final results of an international multicenter, prospective, randomized, controlled trial. Gastrointestinal Endoscopy. 2011; 70(3):465–72. [PubMed: 21741642]
10. Muldoon TJ, Pierce MC, Nida DL, et al. Subcellular-resolution molecular imaging within living tissue by fiber microendosocpy. Opt Exp. 2007; 15:16413–23.
11. Muldoon T, Anandasabapathy S, Maru D, et al. High-resolution imaging in Barrett's esophagus: a novel, low-cost endoscopic microscope. Gastrointestinal Endoscopy. 2008; 68(4):737–44. [PubMed: 18926182]
12. Pierce MC, Vila PM, Polydorides AD, et al. Low-cost endomicroscopy in the esophagus and colon. Am J Gastroenterol. 2011; 106(9):1722–4. [PubMed: 21897416]

13. Aslanoglu M. Electrochemical and spectroscopic studies of the interaction of proflavine with DNA. Anal Sci. 2006; 22(3):439–43. [PubMed: 16733319]
14. Schlemper RJ, Riddell RH, Kato Y, et al. The Vienna classification of gastrointestinal epithelial neoplasia. Gut. 2000; 47(2):251–5. [PubMed: 10896917]
15. Pierce M, Yu D, Richards-Kortum R. High-resolution fiber-optic microendoscopy for in situ cellular imaging. J Vis Exp. 2011; (47):2306. [PubMed: 21248707]
16. Muldoon T, Thekkek N, Roblyer D, et al. Evaluation of quantitative image analysis criteria for the high-resolution microendoscopic detection of neoplasia in Barrett's esophagus. Journal of Biomedical Optics. 2010; 15(2):026027. [PubMed: 20459272]
17. Han JH, Lee J, Kang JU. Pixelation effect removal from fiber bundle probe based optical coherence tomography imaging. Opt Express. 2010; 18(7):7427–39. [PubMed: 20389766]
18. Ljungqvist MG, Nielsen ME, Ersbøll BK, et al. Image analysis of pellet size for a control system in industrial feed production. PLoS One. 2011; 6(10):e26492. [PubMed: 22031836]
19. Sharma P, Savides TJ, Canto MI, et al. The American Society for Gastrointestinal Endoscopy PIVI (Preservation and Incorporation of Valuable Endoscopic Innovations) on imaging in Barrett's Esophagus. Gastrointest Endosc. 2012; 76(2):252–4. [PubMed: 22817781]
20. Pohl H, Rösch T, Vieth M, et al. Miniprobe confocal laser microscopy for the detection of invisible neoplasia in patients with Barrett's oesophagus. Gut. 2008; 57:1648–53. [PubMed: 18755886]
21. Gaddam S, Mathur SC, Singh M, et al. Novel probe-based confocal laser endomicroscopy criteria and interobserver agreement for the detection of dysplasia in Barrett's esophagus. Am J Gastroenterology. 2011; 106(11):1961–8.
22. Wallace M, Sharma P, Lightdale C, et al. Preliminary accuracy and interobserver agreement for the detection of intraepithelial neoplasia in Barrett's esophagus with probe-based confocal laser endomicroscopy. Gastrointestinal Endoscopy. 2010; 72(1):19–24. [PubMed: 20381042]
23. Downs-Kelly E, Mendelin JE, Bennett AE, et al. Poor interobserver agreement in the distinction of high-grade dysplasia and adenocarcinoma in pretreatment Barrett's esophagus biopsies. Am J Gastroenterol. 2008; 103(9):2333–40. [PubMed: 18671819]
24. Gómez V, Buchner AM, Dekker E, et al. Interobserver agreement and accuracy among international experts with probe-based confocal laser endomicroscopy in predicting colorectal neoplasia. Endoscopy. 2010; 42(4):286–91. [PubMed: 20354938]
25. van den Broek FJ, van Es JA, van Eeden S, et al. Pilot study of probe-based confocal laser endomicroscopy during colonoscopic surveillance of patients with longstanding ulcerative colitis. Endoscopy. 2011; 43(2):116–22. [PubMed: 21165821]
26. Muldoon TJ, Roblyer D, Williams MD, et al. Noninvasive imaging of oral neoplasia with a high-resolution fiber-optic microendoscope. Head Neck. 2012; 34(3):305–12. [PubMed: 21413101]
27. Pierce MC, Schwarz RA, Bhattar VS, et al. Accuracy of in vivo multimodal optical imaging for detection of oral neoplasia. Cancer Prev Res (Phila). 2012; 5(6):801–9. [PubMed: 22551901]
28. Quinn MK, Bubi TC, Pierce MC, et al. High-resolution microendoscopy for the detection of cervical neoplasia in low-resource settings. PLoS One. 2012; 7(9):e44924. [PubMed: 23028683]
29. Pierce MC, Guan Y, Quinn MK, et al. A pilot study of low-cost, high-resolution microendoscopy as a tool for identifying women with cervical precancer. Cancer Prev Res (Phila). 2012; 5(11): 1273–1279. [PubMed: 22926339]
30. Shin D, Protano MA, Polydorides AD, et al. Quantitative analysis of high-resolution microendoscopic images for diagnosis of esophageal squamous cell carcinoma. Clin Gastroenterol Hepatol. 10.1016/j.cgh.2014.07.030
31. Vila PM, Kingsley MJ, Polydorides AD, et al. Accuracy and interrater reliability for the diagnosis of Barrett's neoplasia among users of a novel, portable high-resolution microendoscope. Dis Esophagus. 2014; 27(1):55–62. [PubMed: 23442220]
32. Bedard N, Quang T, Schmeler K, et al. Real-time video mosaicing with a high-resolution microendoscope. Biomed Opt Express. 2012; 3(10):2428–35. [PubMed: 23082285]

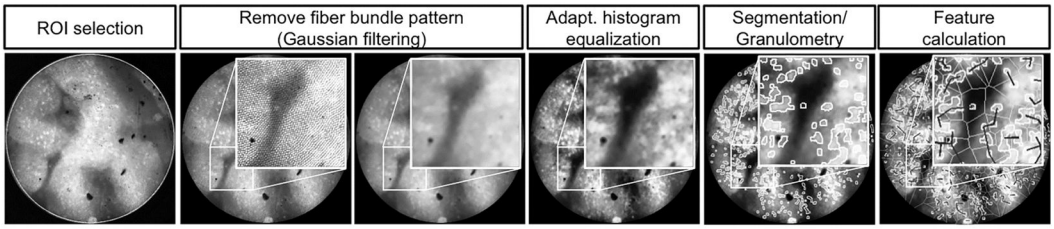

Figure 1.

Image analysis procedure: (A) A circular ROI is selected. (B) Fiber pattern is removed using Gaussian filtering. (C) The contrast of an image is enhanced using adaptive histogram equalization. (D) Nuclei are segmented. The size distribution of glandular features is determined by using granulometry. (E) Quantitative image features are calculated.

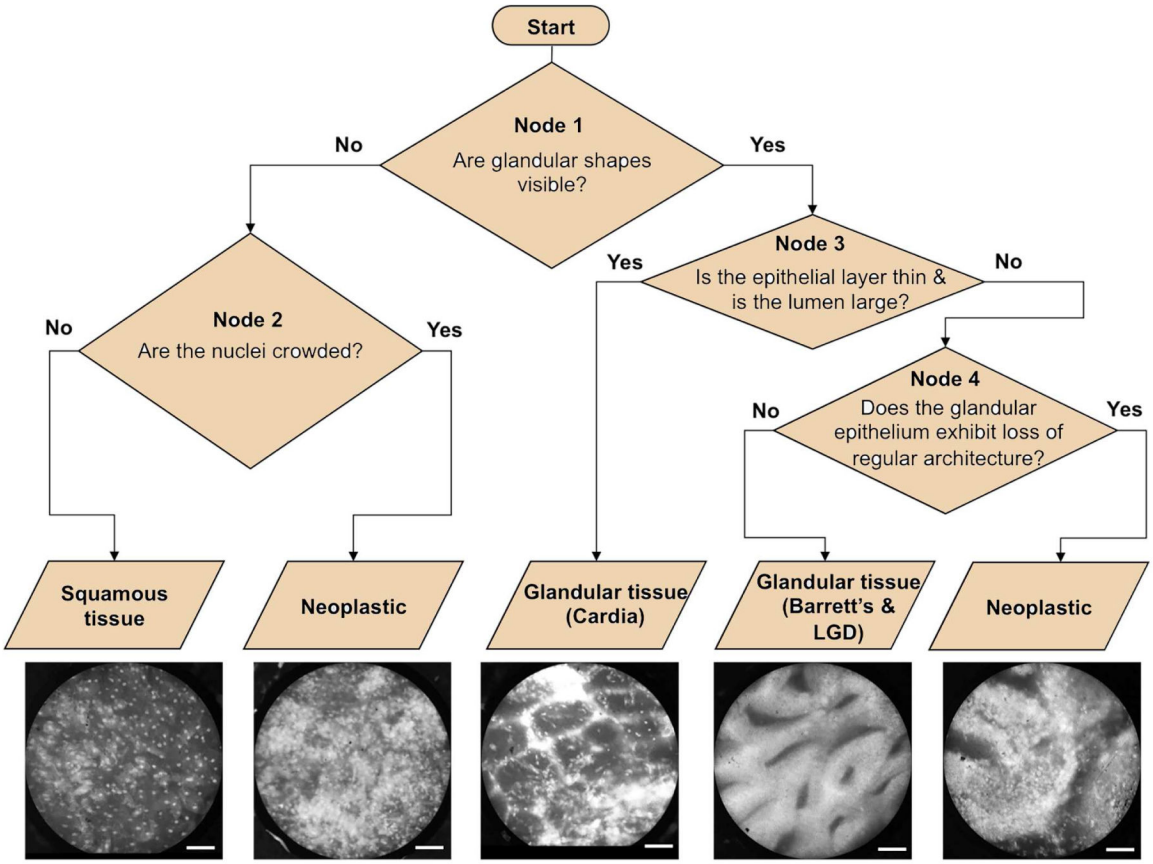

Figure 2.
Flowchart for visual classification. Scale bars represent 100 μm.

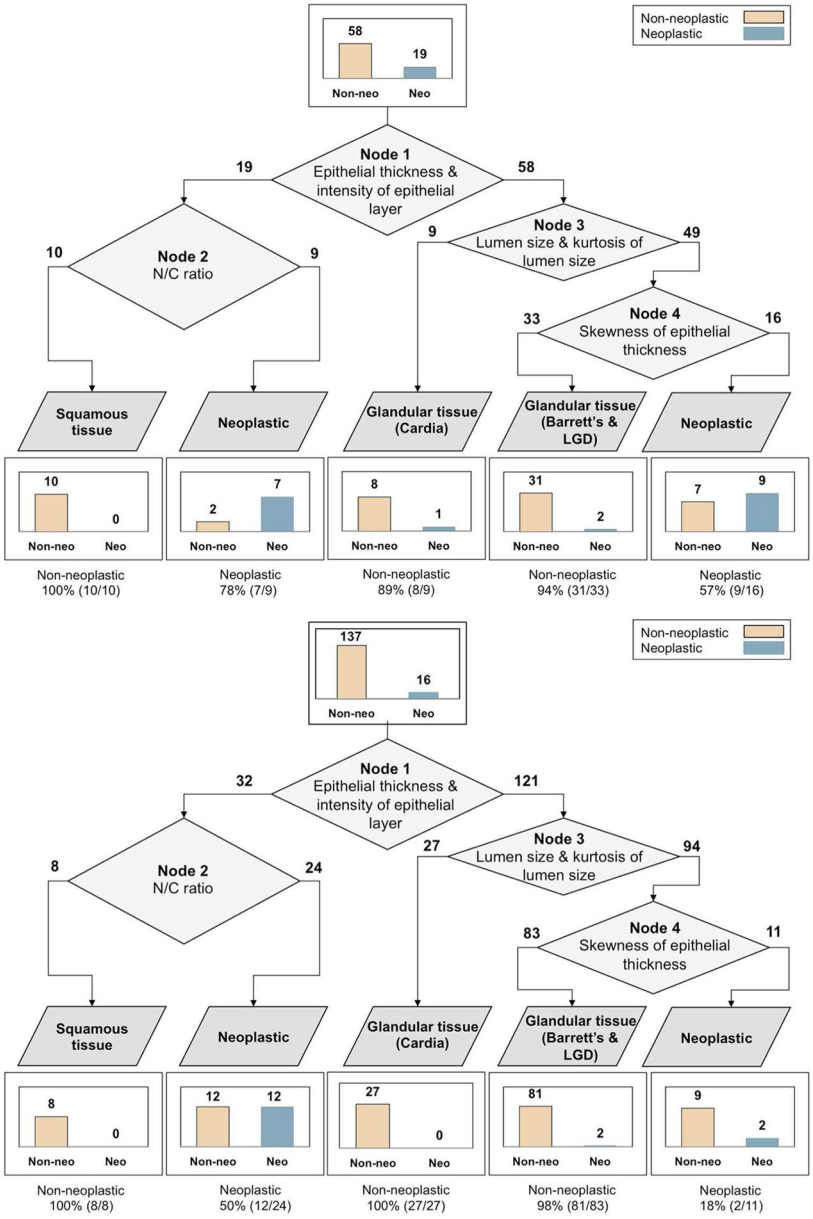

Figure 3.

Resulting classification trees of (A) the training set and (B) the validation set. A bar graph on top indicates the total number of images in the data set. Bar graphs on bottom indicate the number of images classified as one of the categories.

Table 1

Histopathology diagnosis of measured sites.

	Histopathology diagnosis	Training set	Validation set
Non-neoplastic	Squamous mucosa	10	13
	Gastric cardia	14	25
	Barrett's metaplasia	25	85
	Low-grade dysplasia	9	14
Neoplastic	High-grade dysplasia	9	2
	Adenocarcinoma	10	14
	Total	77	153